Supporting Information

Large-Area Silver-Stibnite Nanoporous Plasmonic Films for Label-Free Biosensing

Kandammathe Valiyaveedu Sreekanth, [a, b $] *Weiling Dong,* [c $] *Qingling Ouyang,* [d, e $] *Sivaramapanicker Sreejith,* [f] *Mohamed ElKabbash,* [g] *Chwee Teck Lim,* [f, h] *Giuseppe Strangi,* [g, i] *Ken-Tye Yong,* [*d] *Robert E. Simpson* [*c] *and Ranjan Singh* [*a, b]

[a.] Division of Physics and Applied Physics, School of Physical and Mathematical Sciences, Nanyang Technological University, 21 Nanyang Link, Singapore-637371

[b.] Centre for Disruptive Photonic Technologies, The Photonic Institute, 50 Nanyang Avenue, Singapore-639798

[c.] Singapore University of Technology and Design, 8 Somapah Road, 487372, Singapore

[d.] School of Electrical and Electronic Engineering, Nanyang Technological University, Singapore, 639798

[e.] CINTRA CNRS/NTU/THALES, UMI 3288, Research Techno Plaza, 50 Nanyang Drive, Nanyang Technological University, Singapore, 637553

[f.] Biomedical Institute for Global Health Research and Technology, National University of Singapore, Singapore, 117599.

[g.] Department of Physics, Case Western Reserve University, 10600 Euclid Avenue, Cleveland, OH, 44106 (USA).

[h.] Department of Biomedical engineering, National University of Singapore, Singapore, 117583.

[i.] Department of Physics and CNR-NANOTEC UOS of Cosenza, Licryl Laboratory, University of Calabria, 87036 - Rende (Italy)

* E-mail: robert_simpson@sutd.edu.sg, ktyong@ntu.edu.sg and ranjans@ntu.edu.sg

Methods and Materials

Sample fabrication: Ag-Sb_2S_3 nanoporous samples were prepared on clean BK7 glass substrates by co-sputtering in a magnetic sputtering system (AJA Orion5). Prior to deposition, the BK7 glass substrates were cleaned ultrasonically in acetone, isopropanol and DI water and finally dried with dry Nitrogen. The chamber base pressure was 4×10^{-5} Pa, and the sputtering pressure was 0.5 Pa. The Ag-Sb_2S_3 nanoporous films were co-sputtered using a Sb_2S_3 alloy target and a silver target of diameter 50.8 mm and a purity of 99.99 %. The separation between the substrate and the target was set to 140 mm. The sample holder was kept rotating at a speed of 20 rpm to achieve good uniform samples. The parameters (powers and deposition time) used for the sputtering were listed in the supporting information (Table 1).

Sample characterization: The morphology of the Ag-Sb2S3 nanoporous samples were observed using a Field Emission Scanning Electron Microscope (FESEM, JEOL JSM-7600F). The acceleration voltage was set to 10 kV, and the working distance was set to 7 mm. The compositions of the films were analyzed by energy dispersive x-ray (EDX) spectroscopy in the FESEM. Atomic Force Microscopy (AFM, Asylum Research, MFP-3D Origin) measurements were conducted to obtain the morphology information of the samples in the vertical direction. Tapping mode configuration was used in the measurement. Raman spectra of the Ag-Sb_2S_3 nanoporous films were collected at room temperature in a backscattering geometry using a WITec Alpha300R system. The laser excitation wavelength was 532 nm, and the incident laser intensity was kept at low to minimize irradiation-induced heating of the probed region. The spectral resolution was set to 1.3 cm^{-1}, with spectral range of -16 cm^{-1}~1195 cm^{-1}. Grazing incidence x-ray diffraction (XRD) measurements of the as-deposited Ag-Sb_2S_3 nanoporous films were performed at 1° grazing incidence geometry with

Cu K-α radiation. Diffraction data were collected in 2θ scan mode from 20° to 80° with a step of 0.02°.

Spectroscopic characterizations: Variable-angle high-resolution spectroscopic ellipsometry (J. A. Woollam Co., Inc, V-VASE) was used to determine the thicknesses and optical constants of nanoporous films. The reflectance and transmission spectra as a function of excitation wavelengths were acquired using the same instrument with a wavelength spectroscopic resolution of 2 nm.

Prism coupling experiments: A custom-built angular surface plasmon resonance (SPR) spectroscopy setup was used. A He–Ne laser with a power 4 mW, wavelength 632.8 nm and spot size of around 1 mm^2 was used in the experiment. The prism-coupling configuration was based on the well-known Kretschmann configuration, which includes a BK7 glass right angle prism coupler, which was immobilized on a rotary translation stage. Nanoporous film was attached to the hypotenuse face of the prism with the aid of optical matching oil (Cargille Labs). The intensity of the totally internally reflected light with change in incident angle was collected and monitored through a high-precision optical power meter (Newport 2832C). The reflectance data were calibrated against a highly reflective surface.

Goos–Hänchen shift measurement: In the prism-coupled configuration, *p*-polarized light only enhances the Goos–Hänchen (GH) shift. Therefore, we recorded the differential GH shift between *p*- and *s*-polarized light, which is considered as an optical characteristic carrying the information of the analyte solutions. In particular, *s*-polarized light acts as a reference signal. In the optical setup, light from a He-Ne laser was splitted into *p*- and *s*-polarized light by a polarized beam splitter. An optical chopper was used in the setup so that we can confirm that only one of the beams of *p*- and *s*-polarized light passes through the prism-coupled nanoporous system. The coupling angle was first fixed by rotating the translation stage. The position of the reflected *p*- and *s*-polarized light was then recorded by

using a position sensitive detector (Thorlabs, PDP90A) with a data acquisition card for further processing. Finally, the differential GH shift was obtained after Matlab processing procedures. The noise level of the measurement was less than 0.3 μm.

Analyte preparation: Glycerol solutions with weight percentage concentrations of 1–10 % were prepared in distilled water. Streptavidin (1 mg/mL) was prepared by dissolving 10 mg of the protein in 1 mL distilled water and then diluting in PBS (1:10).

Determination of the optical constants of nanoporous films

Variable angle spectroscopic ellipsometer (J. A. Woollam Co., Inc, V-VASE) was used to obtain the optical constants and thickness of nanoporous thin films. The pair of ellipsometry parameters (Δ and ψ) of nanoporous films with different silver contents were acquired for different incident angles (65°, 70° and 75°) and an oscillator model was used to fit the measured ellipsometry data. For an example, generated and the fitted results of NP sample with silver content 76 at. % are shown in Fig. S1.

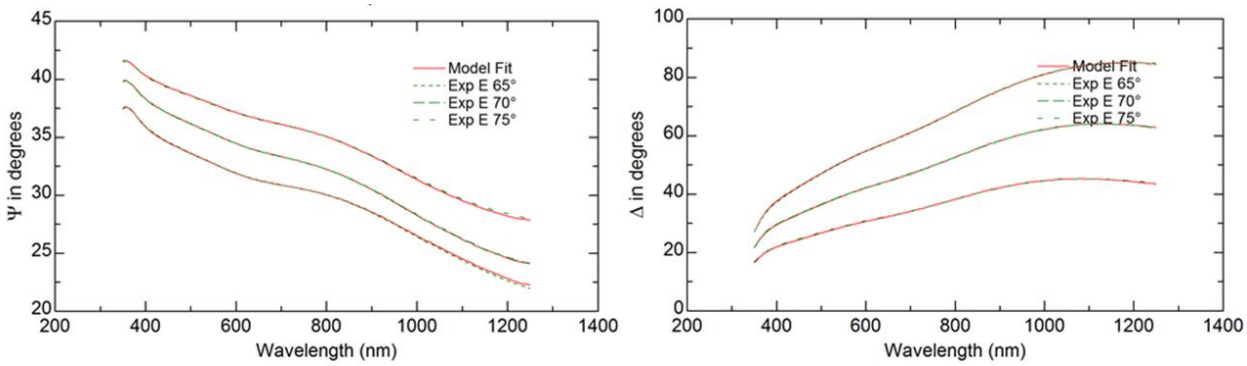

Figure S1 Ellipsometrically generated and fitted results of NP with silver content 76 at. %.

In order to determine the optical constants of Sb_2S_3, an 80 nm thick Sb_2S_3 film was deposited on a clean glass substrate by means of RF sputtering of Sb_2S_3 target and a Gaussian and Lorentz oscillator model was used to fit the measured ellipsometry data. Note that 'as deposited Sb_2S_3 sample' is in amorphous phase. The experimentally acquired optical

constants of Sb_2S_3 (amorphous) are shown in Fig. S2. It is evident that the imaginary permittivity values of Sb_2S_3 are almost zero above 550 nm wavelength, which indicates that Sb_2S_3 is a low-loss chalcogenide material in the visible frequencies.

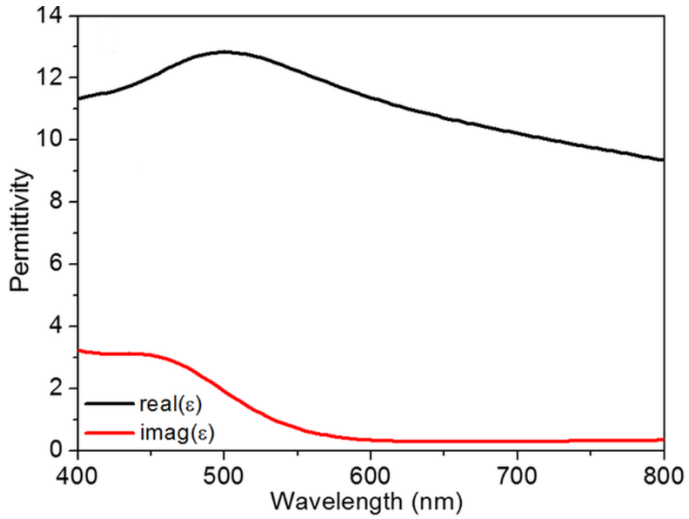

Figure S2 Experimentally determined dielectric constants of Sb_2S_3.

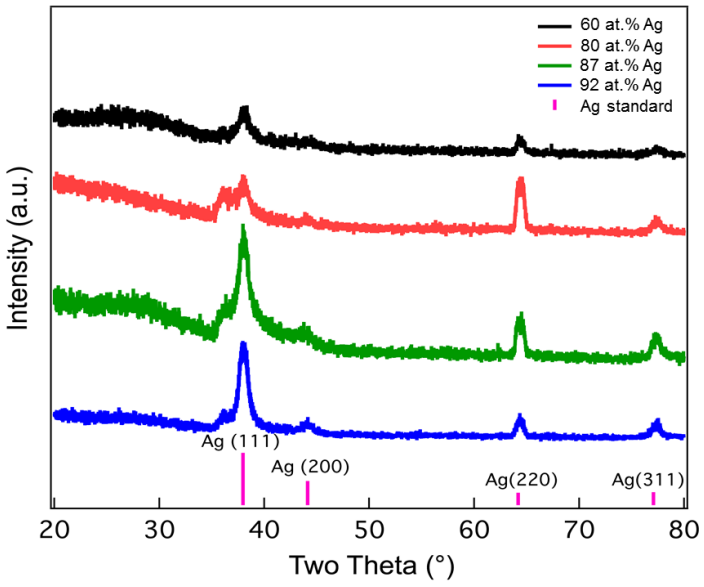

Figure S3 Grazing incidence x-ray diffraction spectra of as-deposited nanoporous films.

Grazing incidence x-ray diffraction (XRD) measurements of the as-deposited Ag-Sb_2S_3 nanoporous films were performed at 1° grazing incidence geometry with Cu K-α radiation. Diffraction data were collected in 2θ scan mode from 20° to 80° with a step of

0.02°. The x-ray diffraction (XRD) spectra of as-deposited nanoporous films are shown in Fig. S3. As can be seen, all four Ag peaks are visible in nanoporous sample with different silver content. The fabrication details of Ag-Sb_2S_3 nanoporous samples are given in Table S1.

Samples	Power of Ag (W)	Power of Sb_2S_3 (W)	Deposition time/s	Ag content (at. %)
1 (Fig. 1a)	30	20	900	60
2(Fig. 1b))	40	20	900	76
3(Fig. 1c)	50	20	900	80
4 (Fig. 1d)	60	20	900	87
5 (Fig. 1e)	80	20	900	92

Table S1: Fabrication details of nanoporous samples with different silver content

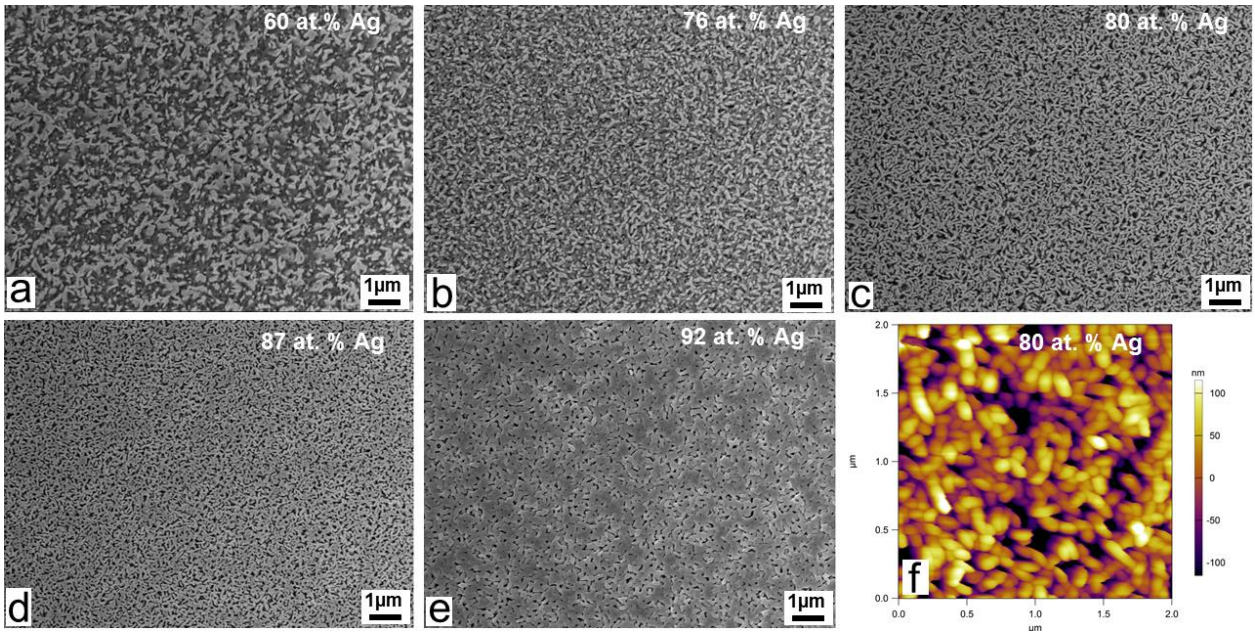

Figure S4 (a-e) SEM images of nanoporous film with different silver contents, (f) Atomic Force Microscopy (AFM) image of nanoporous film with silver content 80 at.%.

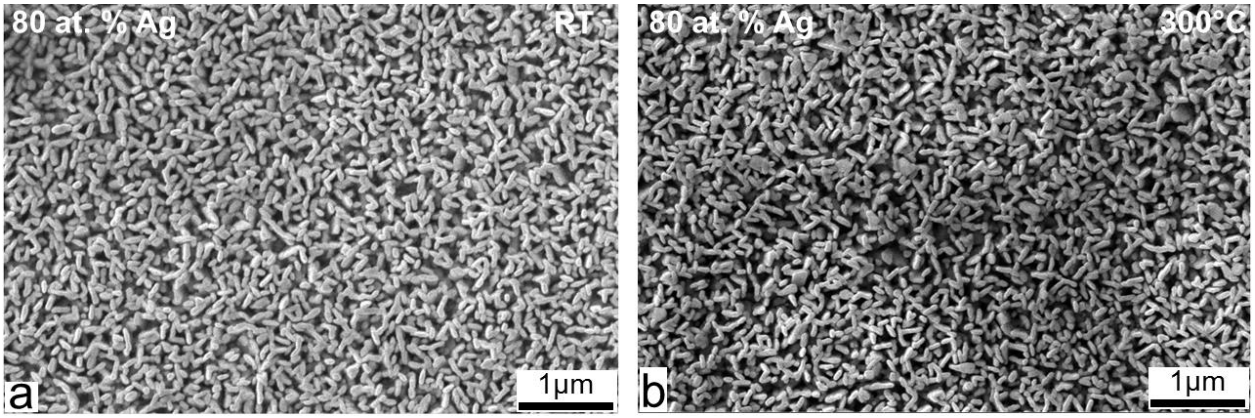

Figure S5 Annealing effect on the morphology of the film. 80 at. % Ag content nanoporous film (a) before and (b) after annealing at 300°C for 2 hr.

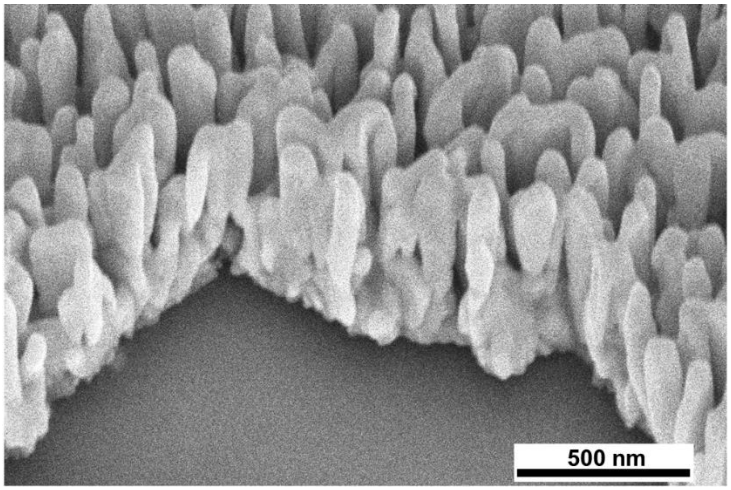

Figure S6 SEM image taken at the edge of a thick nanoporous film (80 at. % Ag) with thickness around 400 nm.

Large area SEM images of nanoporous film with different silver contents are shown in Fig. S4 (a-e). It is clear that pore size decreases with increase in silver concentration. Atomic Force Microscopy image of nanoporous film with silver content 80 at. % is shown in Fig. S4f. The SEM images of 80 at. % silver content NP film before and after annealing at 300°C for 2 hr are shown in Fig. S5a and Fig. S5b, respectively. The SEM image taken at the edge of a 80 at. % Ag nanoporous film with thickness around 400 nm is shown in Fig. S6. This thick NP film was obtained by setting the deposition time at 1800 sec. The tunable

plasmonic response of 80 at. % Ag nanoporous film by varying the deposition time is shown in Fig. S7.

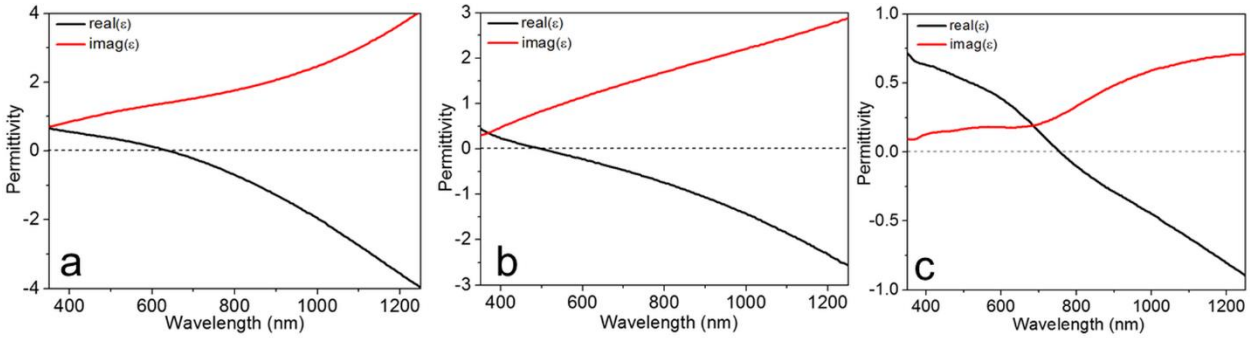

Figure S7 Tunable plasmonic response of the nanoporous (80 at. % Ag) by varying the deposition time (a) 900 sec, (b) 450 sec and (c) 1800 sec.

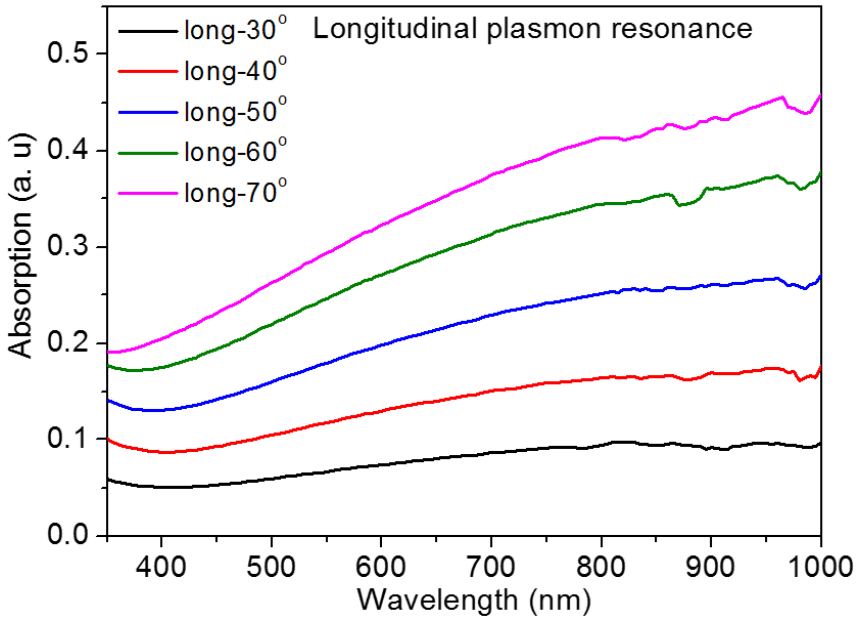

Figure S8 Longitudinal mode absorption spectrum of NP film with silver content 87 at. % for different angles of incidence.

The extracted longitudinal mode absorption by taking the difference between *p*- and *s*-polarized absorption (since it can only be excited by *p*-polarized light) is shown in Fig. S8. As can be seen, it is largely redshifted and it increases with increasing the incident angle,

which indicates that nanoporous has larger component of the *p*-polarization along the long axis of the structure.

Analytical calculations of reflectance, phase shift, GH shift and porosity

In order to obtain a good agreement between the measured and simulated results, the effective dielectric constants of nanoporous layer used in the simulation were obtained using the generalized Maxwell-Garnet approach. Since the Ag-Sb_2S_3 nanoporous films are dominated by silver concentration, we consider the film as Ag nanoporous in the effective dielectric constant calculations. In particular, the nanoporous films used in the experiments have a silver atomic concentration of 87 %. The size of the nanoporous should be much less than the operating wavelength to achieve homogeneity. Since the proposed nanoporous films satisfy this condition, we used a generalized Maxwell-Garnet approach to determine the effective dielectric constants of the films. By assuming that Ag nanoporous is isotopically distributed, the effective dielectric constant of the film is given by[1],

$$\varepsilon_{eff} = \frac{(1+\rho)\varepsilon_m\varepsilon_d + (1-\rho)\varepsilon_d^2}{(1-\rho)\varepsilon_m + (1+\rho)\varepsilon_d} \qquad (1)$$

where ρ is the fill fraction of silver and ε_m & ε_d are the dielectric constants of silver and air.

The reflectance, differential phase and GH shift spectra of the prism-coupled nanoporous system were obtained by solving Fresnel's equations for a three-layer system (prism (1)-NP (2)-air (3)). Reflectance was calculated from, $R_{p,s} = \left| r_{p,s} \right|^2$, where $r_{p,s} = \dfrac{r_{12p,s} + r_{23p,s}\exp(2i\delta)}{1 + r_{12p,s}r_{23p,s}\exp(2i\delta)}$ with $\delta = 2\pi d n_{eff}/\lambda$, d and n_{eff} being the thickness and effective index of the nanoporous film.

For *p*-polarization,

$$r_{jk} = \frac{\left(\frac{k_{zj}}{\varepsilon_j} - \frac{k_{zk}}{\varepsilon_k}\right)}{\left(\frac{k_{zj}}{\varepsilon_j} + \frac{k_{zk}}{\varepsilon_k}\right)} \quad (2)$$

For *s*-polarization,

$$r_{jk} = \frac{\left(\frac{k_{zj}}{\sqrt{\varepsilon_j \varepsilon_k}} - \frac{k_{zk}}{\sqrt{\varepsilon_j \varepsilon_k}}\right)}{\left(\frac{k_{zj}}{\sqrt{\varepsilon_j \varepsilon_k}} + \frac{k_{zk}}{\sqrt{\varepsilon_j \varepsilon_k}}\right)} \quad (3)$$

Thus, the phase angle (ϕ) for both *p*- and *s*-polarization can be obtained from,

$$\phi_{p,s} = \tan^{-1}\left(\frac{\mathrm{Im}(r_{p,s})}{\mathrm{Re}(r_{p,s})}\right) \quad (4)$$

The GH shift for both *p*- and *s*-polarization were calculated by using numerical differentiation of the formula[2],

$$s = -\frac{1}{k}\frac{d\phi_{p,s}}{d\theta} \quad (5)$$

The parameters used in the calculations (Fig. 2 (b, d) & Fig. S9) were,

ρ=0.5 (50%), ε_d=1, ε_m = -3.82001+i*1.34001 (experimentally determined dielectric constant of silver at 632.8 nm), thickness of nanoporous film = 85 nm and the refractive index of prism=1.515 at 632.8 nm.

Dispersion analysis

We find that the nanoporous films show a strong plasmonic response at near infrared (NIR) wavelengths. We simulated the dispersion by calculating the reflectance of a prism-nanoporous-air system as a function of energy and wavevector. The ellipsometrically-derived nanoporous films refractive indices were used to compute and plot the dispersion curve for *p*-polarized, this is shown in Fig. S9a. As can be seen, the area above the air light line

corresponds to surface wavevector values that are radiative on the air side of the interface. The SPP modes exist in the non-radiative region of the dispersion plot and away from the air light line. The minimum reflection lies within the light line gap between the air and the prism. It is clear from the dispersion plot that the nanoporous that containing 87 at. % silver shows a strong plasmonic response for wavelengths λ>1000 nm. Nevertheless, the experimentally determined parallel wavevector of the SPP mode at λ =632.8 nm is 10.02 μm^{-1} (using $(2\pi/\lambda)$ $nsin\theta$ with n being the refractive index of prism and θ being the resonant angle). This value is indicated by a black dot in the dispersion plot in Fig. S9a and lies within the light line gap between the air and the prism. However, the reflected intensity for *s*-polarized light (Fig. S9b) does not show a minimum value within the light line gap at the air-prism interface, which further confirms that the excited mode in the case of *p*-polarization is the SPPs of a nanoporous plasmonic film.

Calculated reflectance, differential phase and GH shift spectra of a prism-NP-water system at 632.8 nm wavelength are shown in Fig. S10. The resonant angle of SPP excitation was determined as around 60° (Fig. S10a). In contrast to GH shifts with air medium (Fig. 3c), the GH shifts obtained with water medium are increased to around 4 times (Fig. S10b) because higher phase change is occurred at the resonant angle. The experimentally determined *p*-polarized reflectance spectrum of prism-nanoporous-water system is shown in Fig. S11. It is evident that the measured SPP resonant angle matches very well with calculated angle.

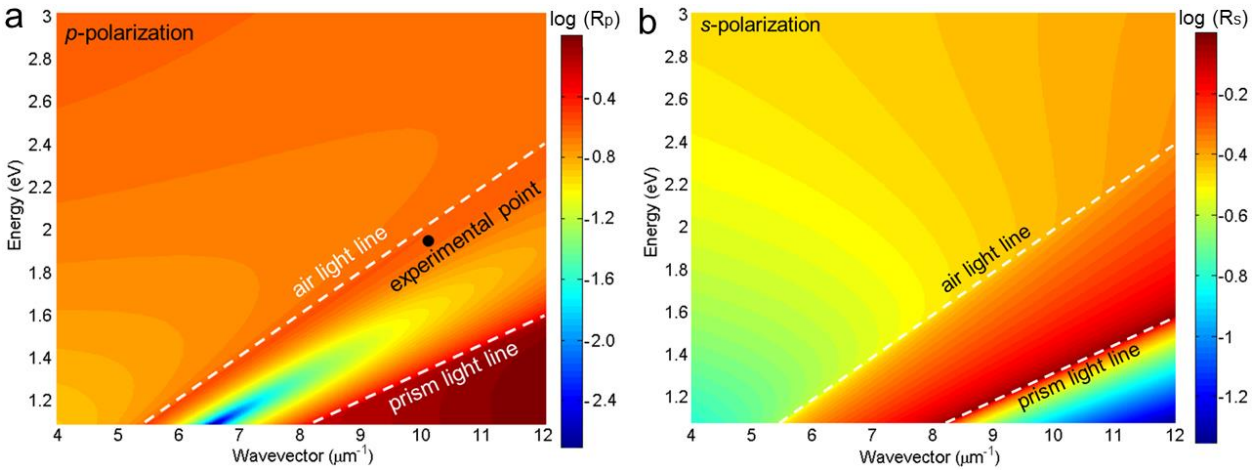

Figure S9 Dispersion plot for (a) *p*-polarization and (b) *s*-polarization.

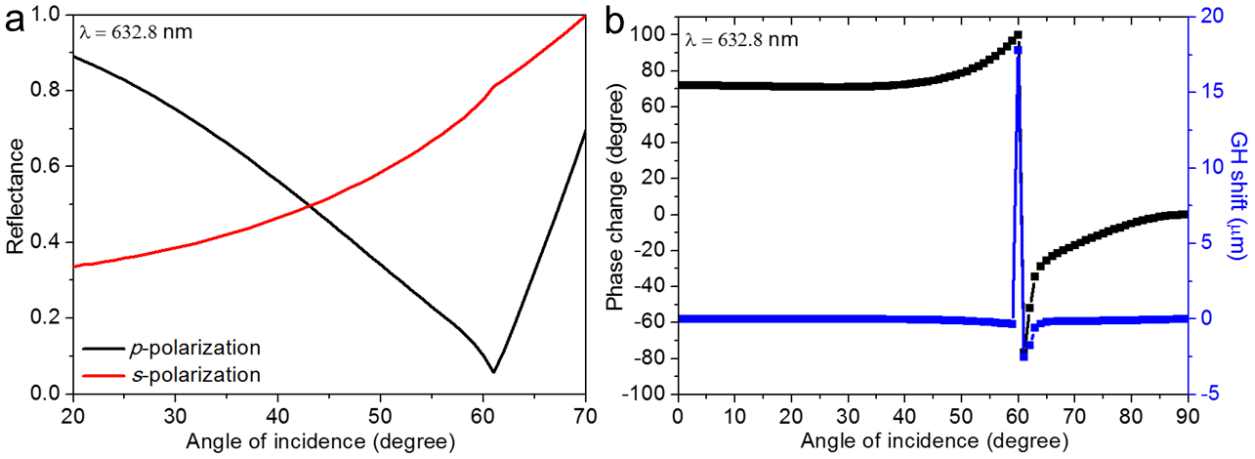

Figure S10 Simulation results of a prism-NP-water system at 632.8 nm. (a) Calculated reflectance spectrum for *p*- and *s*-polarization and (b) Analytically calculated differential phase (black curve) and Goos–Hänchen shift (blue curve) variation as a function of incident angle. Singular phase and maximum GH shift was obtained at the resonant angle.

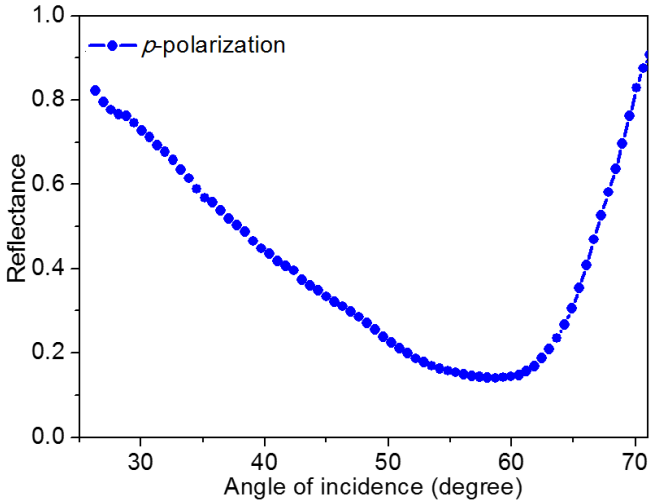

Figure S11 Measured reflectance spectrum of prism-nanoporous-water system at 632.8 nm.

In order to get a best theoretical fit, the parameters used in Fig. 4b were θ=60°, prism index= 1.538 and nanoporous thickness=91 nm and in Fig. 4c were θ=61.5°, prism index= 1.515 and nanoporous thickness=85 nm. The remaining parameters used were, ρ=0.5, ε_d=1 and ε_m = -3.82001+i*1.34001.

Estimation of porosity of the nanoporous films

The average porosity of the porous material can be estimated by using Yoldas's mixing rule[3]. The Yoldas's mixing rule for porous material with air in pores as given by,

$$n_{eff} = \sqrt{((n_{bulk}^2 - 1)(1 - 0.01P) + 1)} \qquad (6)$$

where n_{eff} is the effective refractive index of porous material, n_{bulk} is the refractive index of bulk correspondent material and P is the percentage average porosity of the material. Since we consider the fabricated films as Ag nanoporous films (due to major concentration of silver), the porosity of the fabricated films can be estimated using Yoldas's mixing rule. The estimated percentage porosity of nanoporous with silver content 87 at. % by using the dielectric constants of nanoporous and silver at 632.8 nm wavelength is 58%, which is close

to the fill fraction value that we used in the effective dielectric constants calculation based on Maxwell-Garnet approach.

Bulk refractive index sensing using differential phase measurements

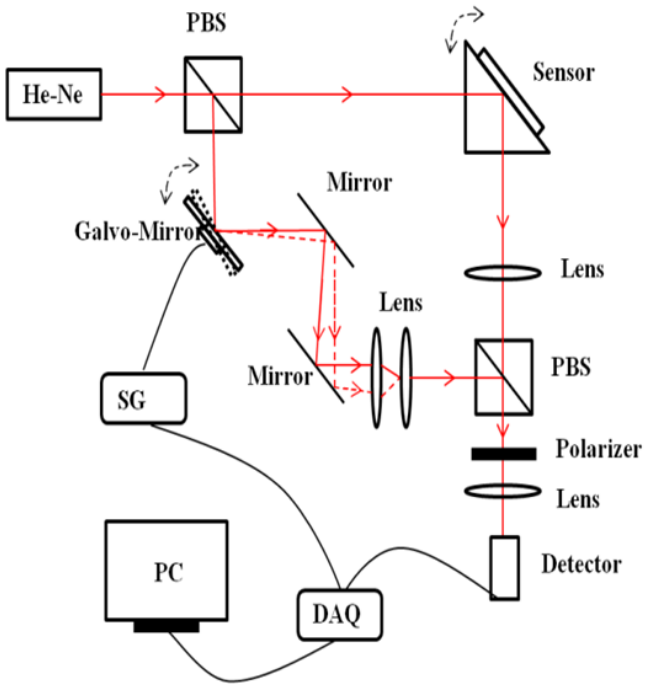

Figure S12 Schematic of experimental setup used for differential phase measurements.

A phase-sensitive SPR setup[4] (Fig. S12) was employed for the experimental investigation of phase change. A 4 mW power and 632.8 nm wavelength He-Ne laser with a beam spot size of 1mm^2 was used to excite the SPP at the nanoporous/water interface. The *p*- and *s*-polarized light were splitted by a polarized beam splitter. In the beam path of *p*-polarized light, the configuration used for the excitation of SPP was based on the well-known Krestchmann configuration, including a right-angle BK7 coupling prism, which was immobilized on a rotation stage. The nanoporous film with a PDMS flow channel (7 x 7 x 2 mm^3) was attached to the face of prism by optical matching oil (Cargille Labs). Sample solutions were injected into the flow channel by a syringe pump to interact with the nanoporous. In the beam path of *s*-polarized light, a galvo-mirror (Thorlabs, GVS001) was

driven by sine wave signals oscillating at 86 Hz to generate optical path difference and to obtain the complete sine waves for the interfering beam of *p*- and *s*-polarized light. The intensity of final interfered light was detected by a photo detector and collected by a data acquisition card (NI PCI-6115) using a Labview program. A point-wise arcsine algorithm was used to extract the phase difference between *p*- and *s*-polarized light.

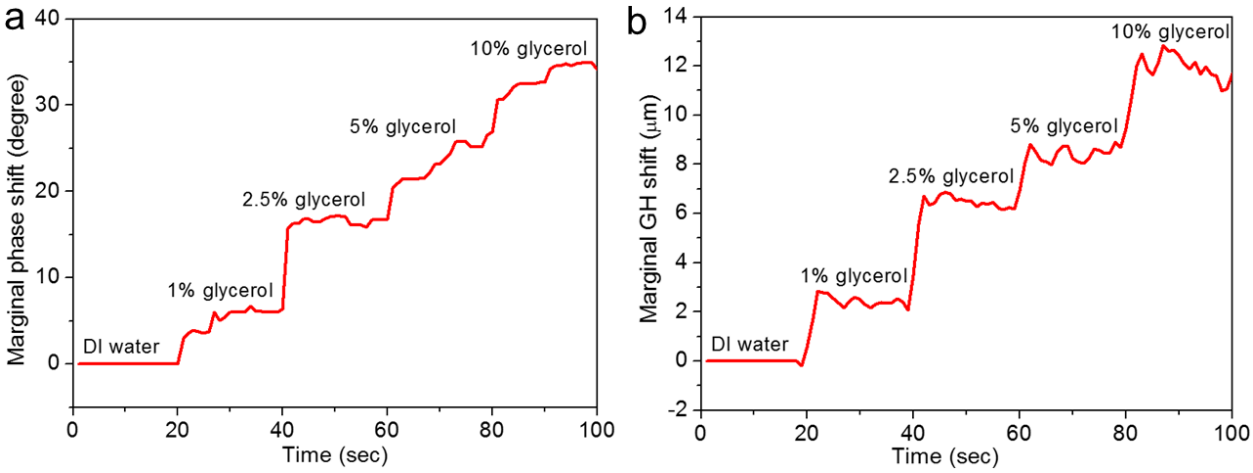

Figure S13 Measured real-time (a) marginal phase shift and (b) marginal GH shift by varying the concentration of glycerol.

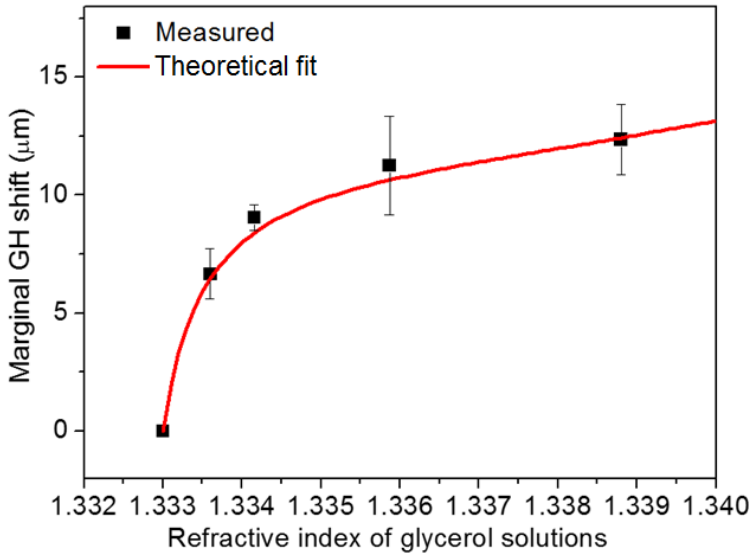

Figure S14 Measured and calculated marginal GH shift variation with refractive index of glycerol

To confirm that prism-coupled nanoporous supports phase singularity at the resonant angle, we studied the relative differential phase shift by setting the angle of incidence at the resonant angle (60°) and varying the external refractive index of the medium. We used different weight percentage ratios of glycerol in DI water (known refractive index liquid) as the sensing medium. The measured real-time differential marginal phase shifts ($\Delta\phi = \left|\phi_{water} - \phi_{glycerol}\right|$) by varying the concentrations of glycerol are shown in Fig. S13a. A clear step in phase shift with increase in glycerol concentration was obtained. The corresponding measured marginal GH shifts ($\Delta S = \left|S_{water} - S_{glycerol}\right|$) step with time by varying the concentration of glycerol (1 % to 10 % w/v) are shown in Fig. S13b. In addition, the results of a control experiment using a 50 nm thick silver film is shown in Fig. S14. In this case, marginal GH shifts variation with refractive index of glycerol solutions were plotted. The best theoretical fit was obtained for the parameters, θ=61.6°, prism index= 1.515, Ag film thickness=51.8 nm and ε_{Ag} = -3.82001+i*1.34001.

Determination of SPP propagation length and penetration depth

Surface plasmon polariton wavevector (k_x) is given by,

$$k_x = k_0\sqrt{\frac{\varepsilon_m\varepsilon_d}{\varepsilon_m + \varepsilon_d}} \qquad (6)$$

Then, the propagation length (L) and effective index (n_{eff}) of the SPP is given by,

$$L = {}^{1}\!\!\diagup\!\!{}_{2\,\mathrm{Im}(k_x)} \text{ and } n_{eff} = {}^{\mathrm{Re}(kx)}\!\!\diagup\!\!{}_{k_0} \qquad (7)$$

The penetration depth (L_z) can be calculated from,

$$L_z = {}^{1}\!\!\diagup\!\!{}_{k_z} \text{ with } k_z = \sqrt{k_x^2 - \varepsilon_m k_0^2} \qquad (8)$$

For nanoporous films, these values were calculated using the experimentally obtained effective dielectric constants of 87 at. % silver content film at 632.8 nm wavelength, which is ε_m = -0.6+i*2.05.

The calculated values for nanoporous-water (ε_d = 1.777) system are: the propagating SPP mode nearest in momentum at resonance is at k_x = 11.58 μm^{-1}, with a propagation length of L =101.5 nm and a penetration depth of L_z = 70.5 nm. The corresponding values calculated for silver-water system at 632.8 nm using ε_{Ag} = -3.82001+i*1.34001 (experimentally obtained) are: the propagating SPP mode nearest in momentum at resonance is at k_x = 16.9 μm^{-1}, with a propagation length of L =242 nm and a penetration depth of L_z = 38.85 nm. It is clear that the propagation length at the silver/water interface is higher than that at the nanoporous/water interface. This is the reason why silver film showed higher bulk refractive index sensitivity compared nanoporous film. However, the penetration depth at the nanoporous/water interface is longer than that at the silver/water interface. This higher penetration depth of nanoporous is useful for improving the surface sensitivity of biomolecules.

Biotin-thiol functionalization on the nanoporous surface

Preparation of biotin disulphide (Product **1)**

In a 100-mL round bottom flask equipped with a magnetic stir bar, biotin (0.28 g, 1.15 mmol) and L-cystine dimethyl ester (0.20 g, 0.06 mmol) were dissolved in dry dichloromethane (DCM) (15 mL) under constant stirring at 600 rpm. *N*-methylmorpholine (NMM) (0.13 mL, 1.18 mmol) was then added to the above mixture, and the mixture was cooled to –10 °C in a salted ice bath (ice + sodium chloride to attain a -10° C temperature). *N*-(3-Dimethylaminopropyl)-*N*′-ethylcarbodiimide hydrochloride **(**EDCl) (0.18 g, 1.16 mmol) was then added to the reaction mixture over 5 min and stirred continuously for another 12 h. The reaction progress was monitored by thin layer chromatography (TLC), and upon completion,

the reaction mixture was quenched using cold 1N hydrochloric acid (HCl) (15 mL) and extracted with DCM. The extract was washed twice with DCM (2 × 20 mL) to ensure the complete extraction of the organic phase. Then, the combined organic phase was washed with brine and dried with anhydrous sodium sulfate (Na_2SO_4), and the solvent was removed under reduced pressure to obtain white solid Product **1** (0.41 g, 69 %). MS (ES): *m*/*z* = 721.5 [M + 1] $^+$.

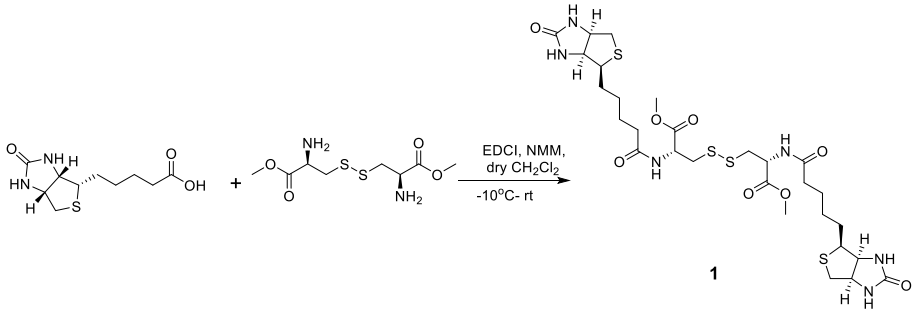

Preparation of biotin-thiol (Product **2)**

To a stirred solution of Product **1** (0.15 g, 0.21 mmol) in anhydrous dimethylformamide (DMF) (4 mL) at ambient temperature under argon atmosphere, tris(2-carboxyethyl) phosphine hydrochloride (TCEP) (0.06 g, 0.25 mmol) was added and dissolved in water (0.4 mL). After 20 h, the reaction mixture was quenched with saturated sodium bicarbonate solution ($NaHCO_3/H_2O$) and extracted with ethylacetate (EtOAc) repeatedly three times. The combined organic layer was washed with brine and dried with anhydrous sodium sulfate (Na_2SO_4), and the solvent was removed under reduced pressure to obtain Product **2** (0.07 g, 93%) as a colorless oil.

The ^{1}H NMR (nuclear magnetic resonance spectroscopy) and mass spectrometry data of Product **2** are: 1H NMR (CD_3OD, 400 MHz): δ = 1.45–1.52 (m, 2 H), 1.61–1.79 (m, 2 H), 2.13–2.24 (m, 1 H), 2.33 (t, 2 H, *J* = 4.0 Hz), 2.61–2.67 (m, 1 H), 2.72 (s, 3 H), 4.39–4.44 (m, 1 H, CH), 2.91 (d, 1 H, *J* = 8.0 Hz), 2.93–2.98 (m, 2 H), 3.15-3.25 (m, 2 H), 4.32-4.37 (m, 1 H), 4.50-4.53 (m, 1 H). MS (ES): *m*/*z* = 362.2 [M + 1]$^+$.

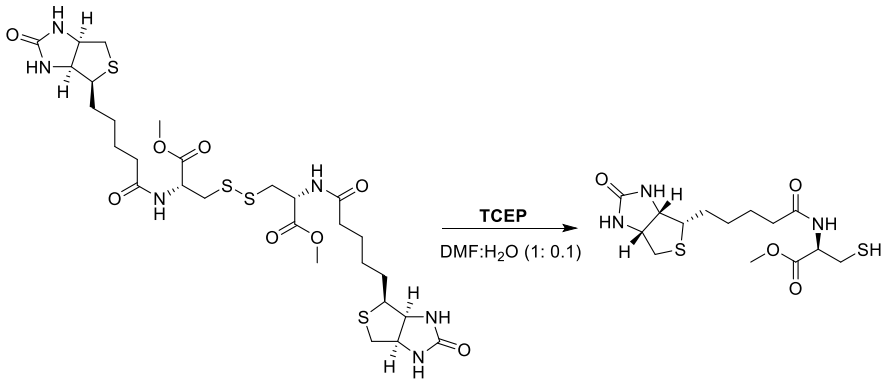

Immobilization of biotin-thiol on Ag-Sb_2S_3 nanoporous surface

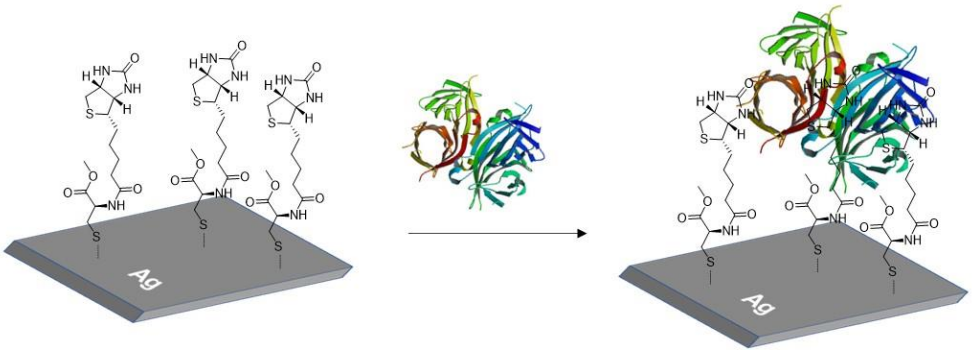

Figure S15 Schematic of biotin-thiol functionalization on nanoporous surface

Ag-Sb_2S_3 nanoporous samples were soaked with solutions of I mM biotin-thiol and kept undisturbed for 24 hours. Surface was cleaned using deionized water and used as such for further analysis. Surface functionalization was further confirmed using XPS analysis by tracing sulfur and nitrogen residues post-modification. The XPS analysis of bare Ag-Sb_2S_3 nanoporous surfaces and biotin-thiol covered Ag-Sb_2S_3 nanoporous surfaces are shown in Fig. S16 and Fig. S17, respectively.

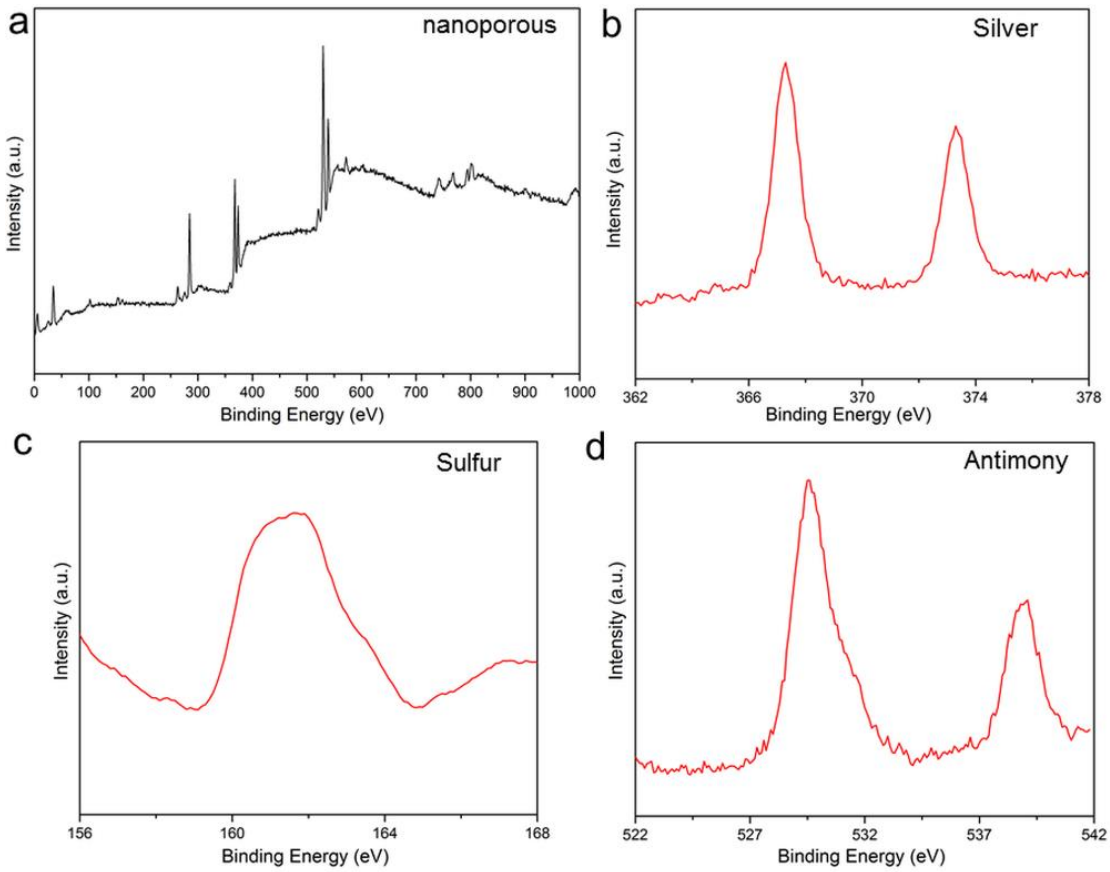

Figure S16 (a) Survey spectrum of Ag-Sb_2S_3 nanoporous film. Elemental spectrum of (b) silver, (c) sulfur and (d) antimony.

The comparison between both spectra are given below,

XPS data of Ag-Sb_2S_3 nanoporous film:

Ag: 367.6 eV ($3d_{5/2}$); 373.6 eV ($3d_{3/2}$); distance between peaks= 6.00 eV

S: 162 eV

Sb: 530.2 eV ($3d_{5/2}$); 539.5 eV ($3d_{3/2}$); distance between peaks= 9.3 eV

XPS data of biotin modified Ag-Sb_2S_3 nanoporous film:

Ag: 369.2 eV ($3d_{5/2}$); 375.2 eV ($3d_{3/2}$); distance between peaks= 6.00 eV

S: 156.5 eV

Sb: peaks can't be find/ merged with oxygen peak

Oxygen: 532.4 eV

Carbon: 284.8 eV

Nitrogen: 400.4 eV

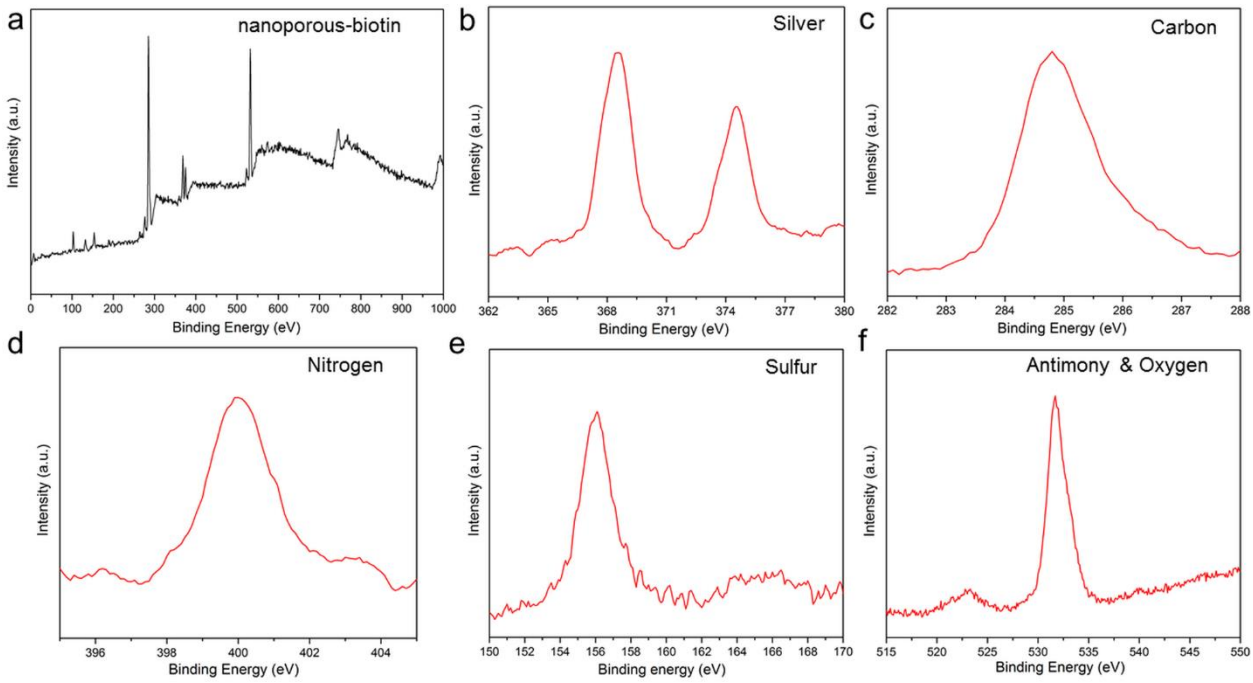

Figure S17 (a) Survey spectrum of biotin covered Ag-Sb_2S_3 nanoporous film. Elemental spectrum of (b) silver, (c) carbon, (d) nitrogen, (e) sulfur and (f) antimony and oxygen.

Experimental GH shift analysis

In glycerol sensing GH shift experiments, we manually injected the DI water into the channel using a syringe and subsequently aqueous solutions of glycerol with different weight ratios (1–10%). The shift was recorded as a function of time (in seconds). The refractive index difference between DI water and 1% glycerol in DI water was used to determine the detection limit of the device. We have repeated the experiments many times and confirmed the reproducibility of the results. The accuracy of the GH shift measurement is around 0.3 µm.

In biosensing experiments, single sample was used to study the binding of different concentrations of streptavidin prepared in PBS. We first recorded the GH shift by injecting PBS (for 5 min), and then injected different concentrations of streptavidin (1 fM to 10 nM), and the corresponding GH shift were recorded with progress in time. Finally, PBS was again injected into the channel after a reaction time of 30 min to remove unbound and weakly attached streptavidin molecule. We then calculated marginal GH shift, i.e.

$\Delta S = \left| S_{pbs} - S_{streptavidin} \right|$. We observed a discrete step in the GH shift over time, which is a clear signature of the binding of individual streptavidin molecules on the sensor surface. We have repeated this study for all concentrations of biotin using different samples from the same batch and noticed that GH shift varied from sample to sample. Therefore, the corresponding error bar is obtained and plotted along with the data.

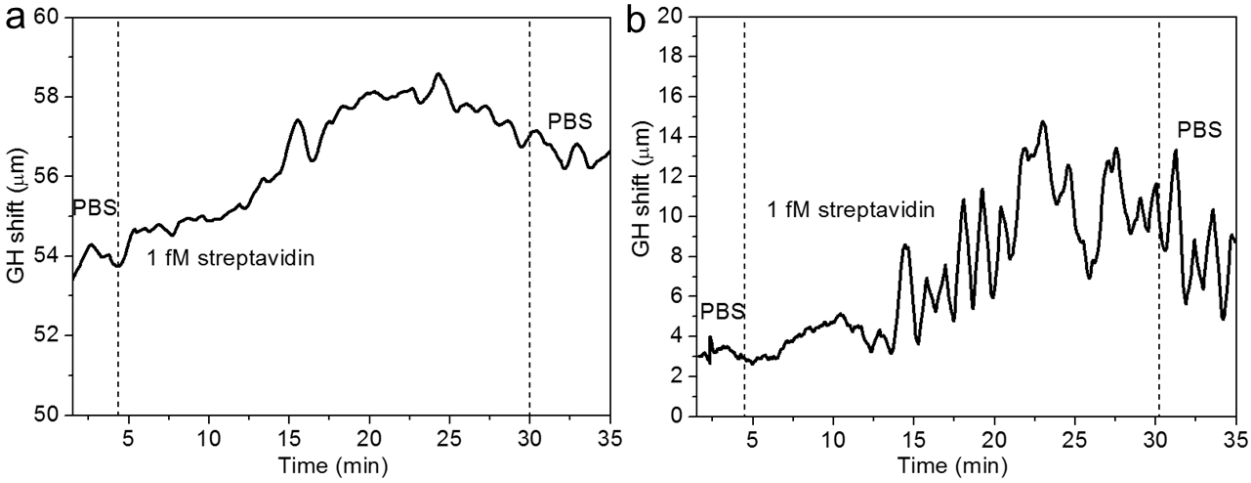

Figure S18 Biosensing results of control experiments. Real time binding response of the sensor by injecting 1 fM streptavidin concentration in PBS with time. Raw data of the absolute GH shift of (a) biotin functionalized silver film and (b) unfunctionalized nanoporous film.

The control experiments for 1 fM streptavidin concentration using biotin functionalized 50 nm thick silver sample and bare nanoporous sample were performed. The raw data of absolute GH shift over time is presented in Fig. S18. The specific binding of streptavidin molecules over time is evident in the case of functionalized silver sample (Fig. S18a). However, the recorded shift is negligible compared to functionalized nanoporous sample. From the raw data of unfunctionalized nanoporous sample (Fig. S18b), it is clear that both specific and unspecific binding events are occurred over time. In contrast to control

experimental results, the functionalized nanoporous samples showed significant step in GH shift over time, which is a clear signature of the specific binding events.

Estimation of highest number of adsorbed molecules

Here, we used the similar approach proposed in ref [5] for estimating the adsorbed molecules on the sensor surface. Since the illuminated beam diameter is around 1mm^2, the effective sensor area is 1 mm^2 and the adsorbed molecules are equally distributed across the entire sensor surface, which has a dimension of 7 mm x 7 mm, an area of 49 mm^2. Hence, given a certain maximum possible adsorbed population on the surface, only a fraction 1 mm^2 /49 mm^2 = 0.02 (2%) will be in the sensing region and relevant to the GH shift.

Since the PDMS channel has a height of 2 mm, initially there are c (7 mm x 7 mm x 2 mm/1L) M^{-1} = 5.9 c x 10^{19} M^{-1} biomolecules in solution inside the device. In the long-time limit, if all of these were to be adsorbed irreversibly on the sensor surface, on average 2% of the total would be in the sensor areas. Thus:

$$N_{\max}(c) = 11.8\, c \times 10^{17}\ \mathrm{M}^{-1}$$

For 1 fM streptavidin solution, $N_{\max}$ = 1180. This value could be the maximum number of molecules adsorbed on the sensor surface.

References

(1) Cortes, C. L.; Newman, W.; Molesky, S.; Jacob, Z. Quantum Nanophotonics using Hyperbolic Metamaterials. *J. Opt.* **2012**, 14, 063001.

(2) Liu, X.; Cao, Z.; Zhu, P.; Shen, Q.; Liu, X. Large Positive and Negative Lateral Optical Beam Shift in Prism-Waveguide Coupling System. *Phys. Rev. E.* **2006**, 73, 056617.

(3) Yoldas, B. E. Investigations of Porous Oxides as an Antireflective Coating for Glass Surfaces. *Appl. Opt.* **1980**, 19, 1425-1429.

(4) Zeng, S.; Sreekanth, K. V.; Shang, J.; Yu, T.; Chen, C.-K.; Yin, F.; Baillargeat, D.; Coquet, P.; Ho, H.-P.; Kabashin, A. V.; Yong, K. –T. Graphene-Gold Metasurface Architectures for Ultrasensitive Plasmonic Biosensing. *Adv. Mater.* **2015**, 27, 6163-6169

(5) Sreekanth, K. V.; Alapan, Y.; ElKbbash, M.; Ilker, E.; Hinczewski, M.; Gurukan, U. A.; De Luca, A.; Strangi, G. Extreme Sensitivity Biosensing Platform Based on Hyperbolic Metamaterials. *Nat. Mater.* **2016**, 8, 621-627.